AER/AGS Special Report 116

# Analysis of WorldView-3 Satellite Imagery for the Leland Lakes Area, Alberta

AER/AGS Special Report 116

# Analysis of WorldView-3 Satellite Imagery for the Leland Lakes Area, Alberta

B. Rivard

Department of Earth and Atmospheric Sciences, University of Alberta

November 2023

©His Majesty the King in Right of Alberta, 2023
ISBN 978-1-4601-5707-7

The Alberta Energy Regulator / Alberta Geological Survey (AER/AGS), its employees and contractors make no warranty, guarantee, or representation, express or implied, or assume any legal liability regarding the correctness, accuracy, completeness, or reliability of this publication. Any references to proprietary software and/or any use of proprietary data formats do not constitute endorsement by the AER/AGS of any manufacturer's product.

If you use information from this publication in other publications or presentations, please acknowledge the AER/AGS. We recommend the following reference format:

Rivard, B. (2023): Analysis of WorldView-3 satellite imagery for the Leland Lakes area, Alberta; Alberta Energy Regulator / Alberta Geological Survey, AER/AGS Special Report 116, 23 p.

Publications in this series have undergone only limited review and are released essentially as submitted by the author.

**Author address:**
B. Rivard
Department of Earth and Atmospheric Sciences
University of Alberta
1-26 Earth Sciences Building
Edmonton, AB  T6G 2E3
Canada

Tel: 780.953.7110
Email: bentrivard9@gmail.com

**Published November 2023 by:**
Alberta Energy Regulator
Alberta Geological Survey
Suite 205, 4999 – 98 Avenue NW
Edmonton, AB  T6B 2X3
Canada

Tel: 780.638.4491
Email: AGS-Info@aer.ca
Website: ags.aer.ca

# Foreword

As part of the Alberta Minerals Strategy and Action Plan, the Alberta Energy Regulator (AER) / Alberta Geological Survey (AGS) acquired Maxar WorldView-3 satellite imagery over the Canadian Shield (the Shield) in northeastern Alberta. This acquisition was to support the detection and mapping of metallic mineral occurrences in the Shield, where known occurrences of gold, base metals, uranium, and rare-earth elements have been previously documented in narrow belts surrounding several major shear zones.

In March 2022, Professor Emeritus Benoit Rivard was contracted to conduct a preliminary analysis on the WorldView-3 satellite imagery of the Leland Lakes area in northeastern Alberta. This contract was awarded as part of the Mineral Grant provided by the Government of Alberta on June 22, 2021. The primary objective was to identify potential mineral occurrences in the Alberta Shield region by detecting exposed rock outcrop, delineating lithological units, and mapping mineral alteration.

This report describes the results of this preliminary analysis, which focusses on the preprocessing methods required to isolate pure pixels of rock outcrop in the imagery and to mask non-rock features such as vegetation, water, and shadows. The report also includes the findings from an initial analysis of the spectra of these rock surfaces in terms of detecting iron- and hydroxyl-bearing minerals and distinguishing between mafic and felsic lithological domains.

Aside from the cover, copyright information, and this page, the report is published as received from the vendor (with minor editing).

# AER Service Agreement 22SA-SR003

Analysis of WorldView-3 satellite imagery for the Leland Lakes area, Alberta

By

Professor Emeritus Benoit Rivard
bentrivard9@gmail.com, 780-953-7110

March 28, 2023

## Contents



## Figures

## Appendices

# 1 INTRODUCTION

This report summarizes the analysis of Maxar WorldView-3 imagery over the Leland Lakes area of interest in Alberta as part of AER Service Agreement 22SA-SR003. The area encompasses extensive vegetation cover, and the analysis aimed to isolate exposed outcrop, delineate lithological units, and detect and map potential mineral alteration. The limited spectral dimensionality of WorldView-3 data implied a focus on the detection of iron oxides and clay alteration. This work is conducted as part of an initiative to detect potential metallic mineral occurrences in the Alberta Shield, where known occurrences of gold, base metals, uranium, and rare-earth elements have been documented in narrow belts surrounding several major shear zones (Langenberg et al., 1994). These mineral occurrences are associated with alteration mineral exposures on the surface, such as weathered sulphide horizons, quartz-tourmaline metasediments, and pegmatites.

# 2 SATELLITE DATA

Three lines of WorldView-3 satellite data acquired on September 22, 2022, largely encompass the area of interest in northern Alberta, shown in Figure 1. Each line was delivered as two datasets. The visible near infrared data (VNIR) has eight spectral bands located nominally at 425, 480, 545, 605, 660, 725, 832, and 950 nm with a spatial resolution of 1.24 m. The shortwave infrared data (SWIR) has eight spectral bands located nominally at 1210, 1570, 1660, 1730, 2165, 2205, 2260, and 2330 nm with a spatial resolution of approximately 4 m. Preprocessing of the data conducted by the data provider included an atmospheric correction (ACOMP) with the Single Channel Algorithm (SCA) correction applied to both datasets to minimize stripping, a standard orthorectification with nearest neighbour resampling, and an alignment correction (i.e., a boresight correction) for both datasets to enable their joint analysis. The data delivered is thus orthorectified imagery with at-surface reflectance, and the SWIR data is resampled to 1.24 m to provide a 16-band spectrum per 1.24 m pixel. Figure 2 is a 'true colour' mosaic (863 km$^2$) of the three lines encompassing the area of interest.

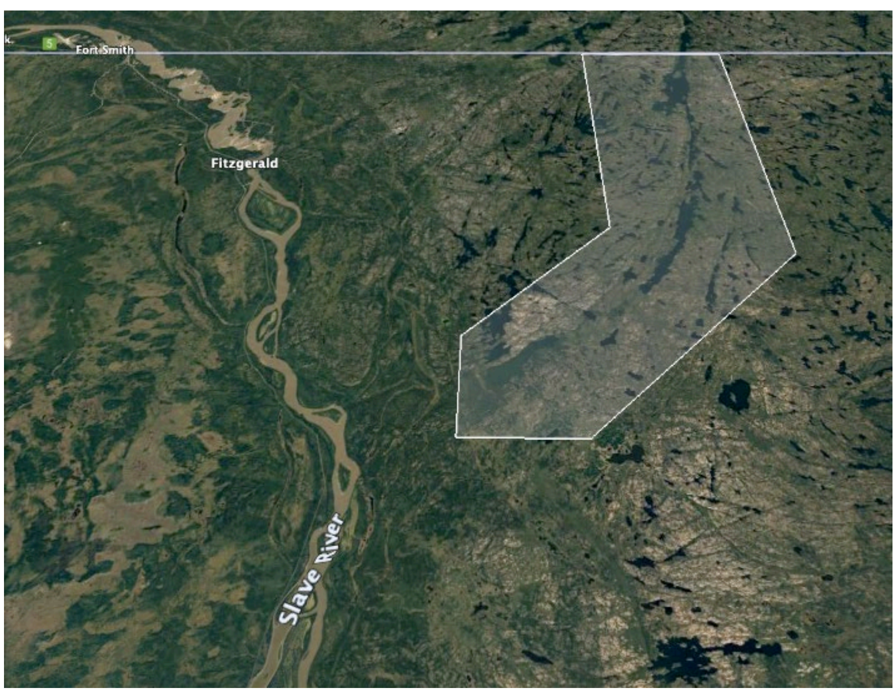


**Figure 1. Google Maps view with a white polygon defining the area of interest encompassed by the satellite data.**

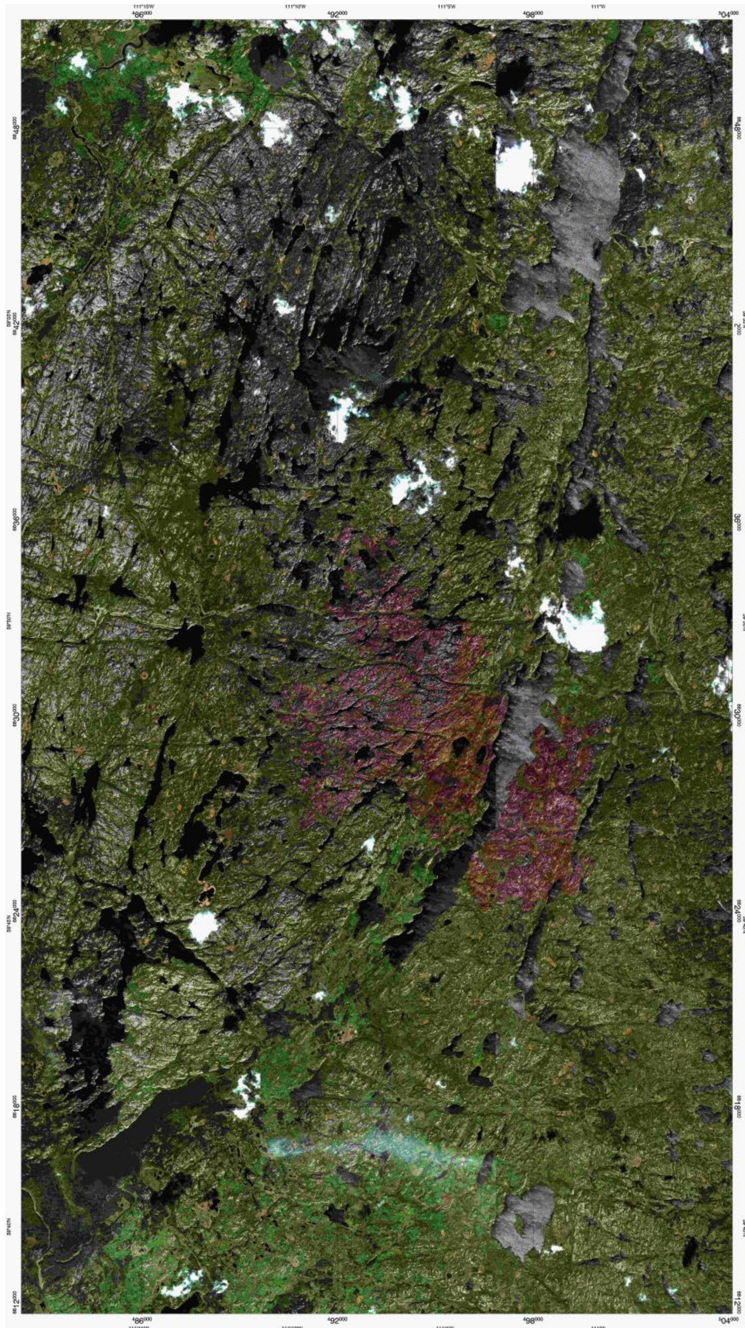

**Figure 2. 'True colour' mosaic of the three lines of WorldView-3 satellite data encompassing the area of interest. White clouds are visible, as well as a fire scar (red).**

Despite the corrections listed above, there remains a misalignment of VNIR and SWIR data noted on the borders of each line, most prominently on the left side. An example is shown in Figure 3 in the northwestern corner of one line. Consequently, when the mosaic of the three lines was assembled for varying products, 356 pixels (or 441 m) we truncated on each side of each line prior to assembly of the mosaic. This ensured removal of alignment errors in the mosaic and derived products.

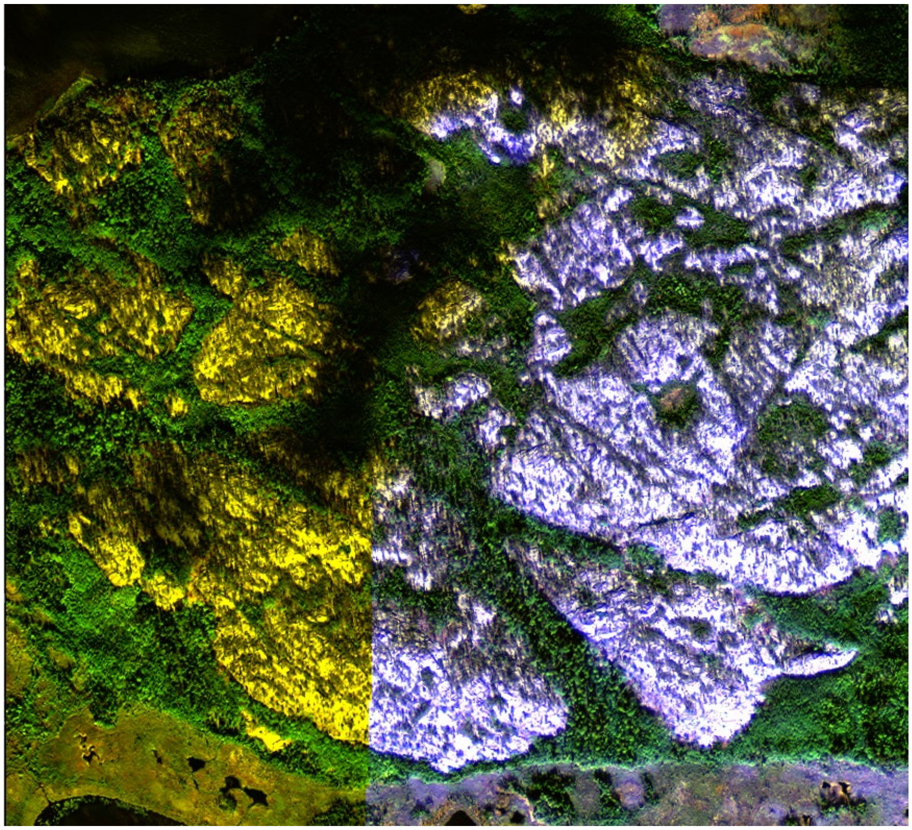

**Figure 3. Example misalignment of VNIR and SWIR data seen on the left side for a colour composite (R=660 nm, G=545 nm, B=2205 nm) of the northwestern corner of line WV3 22Sept11184747-M3DM R01C1-RT_92647_3010_01_P001-003.**

# 3 METHODS

Several methods were used, first to isolate pixels of bedrock outcrop, and then to extract lithological information. The first category involves masking all pixels not occupied by outcrop, which includes pixels affected by clouds, water, vegetation, burns, and shadows. The second category includes the extraction and analysis of spectral endmembers as well as spectral indices.

## 3.1 Masking

Three masks (Equations 1–3) were designed for masking vegetation, clouds, water, burns, and shadows. A normalized vegetation index (NDVI; Equation 1) was calculated for every pixel in the VNIR data to mask standing water (e.g., lakes, rivers), vegetation, and clouds. The Shadow index (Equation 2; Shedlovska and Hnatushenko, 2019) and Burn index (Equation 3) minimize the impact of shadows (including cloud shadows) and recent fire scars.

Equation (1) NDVI index = (VNIR 7 – VNIR 5) / (VNIR 7 + VNIR 5)

Equation (2) Shadow index = (VNIR 8 – VNIR 2) / (VNIR 8 – VNIR 2) – VNIR 7

Equation (3) Burn index = (VNIR 1 + VNIR 2 + VNIR 3) / 3

#### *3.1.1 For the generation of an outcrop map*

To derive an outcrop distribution map, the following thresholds were used: pixels were retained if the NDVI was >0.01 but <0.4, the Burn index was >0.06, and the Shadow index was <0.5.

#### *3.1.2 For the generation of lithological information*

Prior to the extraction of lithological information from pixels occupied by outcrop, further masking was applied to the outcrop map. Our rationale is that the primary value of the outcrop map to geologists is for logistical planning of fieldwork, and thus the map could encompass pixels partially occupied by outcrop (e.g., mixed with vegetation and shadow), whereas the extraction of lithological information should be pursued from a more conservative outcrop map, where the effects of vegetation and shadows are at a minimum. Therefore, pixels were retained if the NDVI was >0.01 but <0.35, the Burn index was >0.07, and the Shadow index was <0.4.

### 3.2 Endmember extraction

The use of spectral endmembers is one approach to explore the data for lithological information. Endmembers represent 'purest' spectra of representative materials in the scene. Endmembers can be collected in the field or laboratory from known surfaces (outcrop or samples, respectively) or extracted from imagery. The latter is commonly preferred for two reasons: (1) laboratory and field spectra may not capture all relevant surface components or may be inadequate representations (e.g., fresh rather than exposed weathered surfaces), and (2) image endmembers sample surfaces directly from the scene and are collected under the same viewing and illumination conditions as all spectra in the scene. Image endmembers are assumed to be relatively pure spectra, meaning that minimal mixing with other endmembers has occurred within the pixel.

To derive an image endmember set from the satellite data, we used the spatial-spectral endmember extraction (SSEE) method described in Rogge et al. (2007, 2012). The number of endmembers extracted by the SSEE method is defined by the data. The SSEE method comprises three steps. The image is first divided into equal-sized non-overlapping subset regions and a set of eigenvectors that explain the majority of spectral variance is calculated for each subset via singular value decomposition. In the second step, the image data are projected onto the local eigenvectors compiled from all subset regions and those pixels that lie at extremes of the vectors are retained as candidate endmembers. The third step averages the candidate pixels with all other pixels within a given spatial window that are also spectrally similar based on a similarity metric, such as spectral angle (Price, 1994). The SSEE method generally finds several endmembers and many that are similar but spatially independent. Fifteen geologically relevant endmembers were obtained and are shown in Figure 4. As discussed in the results, these were examined, and we selected three endmembers as input to the Spectral Angle Mapper (SAM) tool to capture what appeared to be spatially continuous and significant areas (e.g., lithological units). Most of the endmembers seen in Figure 4 are spectrally similar, varying primarily in overall amplitude. Importantly, because all 16 bands were used in this endmember search, the discriminating influence of absorption features attributable to hydroxyl ($OH^-$)- and iron-bearing minerals is lost. Therefore, as described in the next section, we also pursued the use of indices capturing mineralogical information based on specific subsets of bands for a given absorption feature.

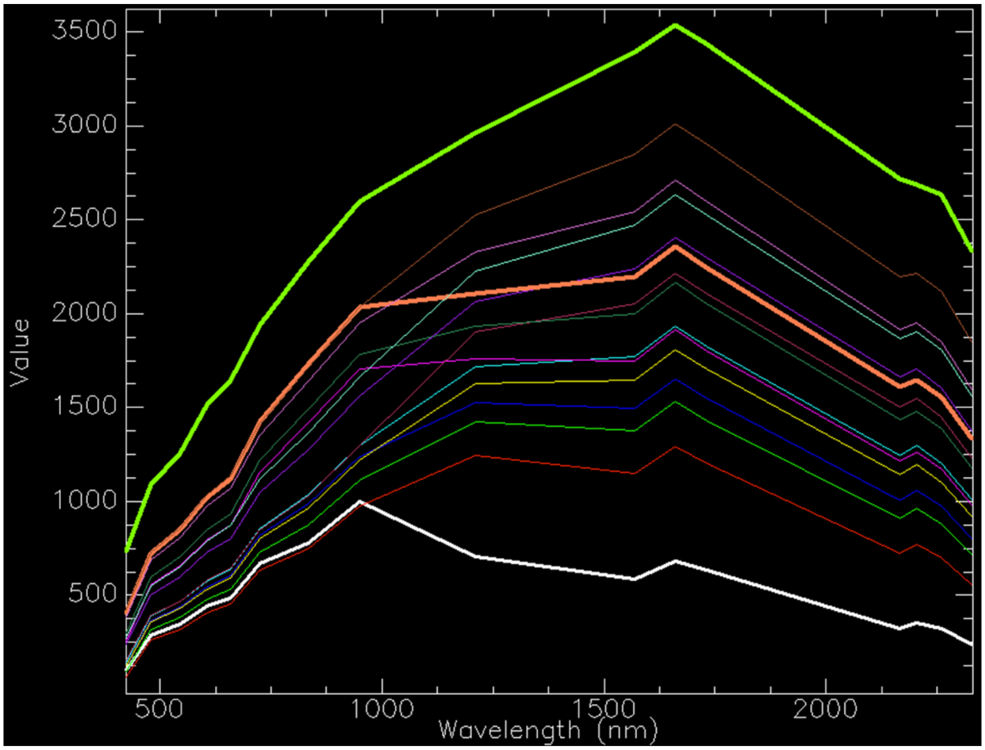


**Figure 4. Spectra of 15 endmembers were obtained from the endmember extraction process using all 16 available bands. Wavelengths in nm and reflectance x 100 (i.e., 1000=10%). Endmembers 15 (green), 11 (orange), and 1 (white) are highlighted with thicker lines because they were used to derive specific image products.**

## 3.3 Indices

Three indices were devised to capture mineralogical and, thus, lithological information related to the presence of hydroxyl ($OH^-$)– and iron ($Fe^{3+}$)–bearing minerals (e.g., clays and iron oxides) seen in WorldView-3 image spectra (Figure 5).

The 'White mica index' is listed in Equation 4 and consists of a normalized ratio of two bands (SWIR 5, SWIR 6) at 2164 and 2202 nm, respectively, and thus capitalizes on the white mica absorption feature located nominally at 2200 nm. It is used with the intent to inform on the relative abundance of white mica. The 'Rock MF (Mafic Felsic)' index and the 'Rock Fe (iron)' index are listed in Equations 5 and 6, respectively. The Rock Fe index is designed specifically to measure the strength of the iron absorption nominally centred on band VNIR 7 located near 900 nm.

Equation (4) White mica index = (SWIR 5 – SWIR 6) / (SWIR 5 + SWIR 6)

Equation (5) Rock MF index = (VNIR 3 + SWIR 3) / (VNIR 5 + VNIR 7)

Equation (6) Rock Fe index = ((VNIR 6 – VNIR 7) / (VNIR 6 + VNIR 7)) + ((VNIR 8 – VNIR 7) / (VNIR 8 + VNIR 7))

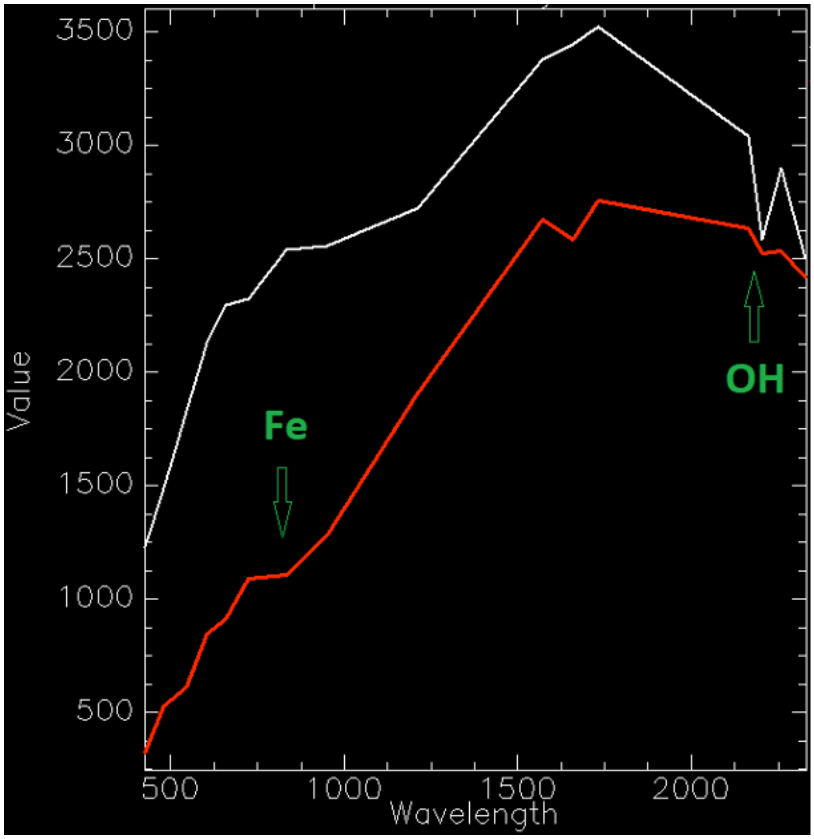


**Figure 5. Example of WorldView-3 spectra showcasing a strong iron (Fe) absorption near 900 nm (red spectrum) and a strong hydroxyl ($OH^-$) absorption near 2200 nm (white spectrum).**

# 4 RESULTS

## 4.1 Outcrop map

A portion of the bedrock outcrop map generated for one WorldView-3 line is shown in Figure 6 to illustrate the output compared to a 'true colour' WorldView-3 image where water, clouds, and vegetation are present. Note that the vegetation threshold selected should imply less than approximately 30% leafy vegetation within a pixel. The methodology implemented aims to provide field geologists with a realistic map of outcrop distribution for the planning of fieldwork. The outcrop map for the full area of interest (e.g., the mosaic) is shown in Figure 7 and can be compared to that used for the lithological analysis (e.g., input to indices), also shown in the same figure.

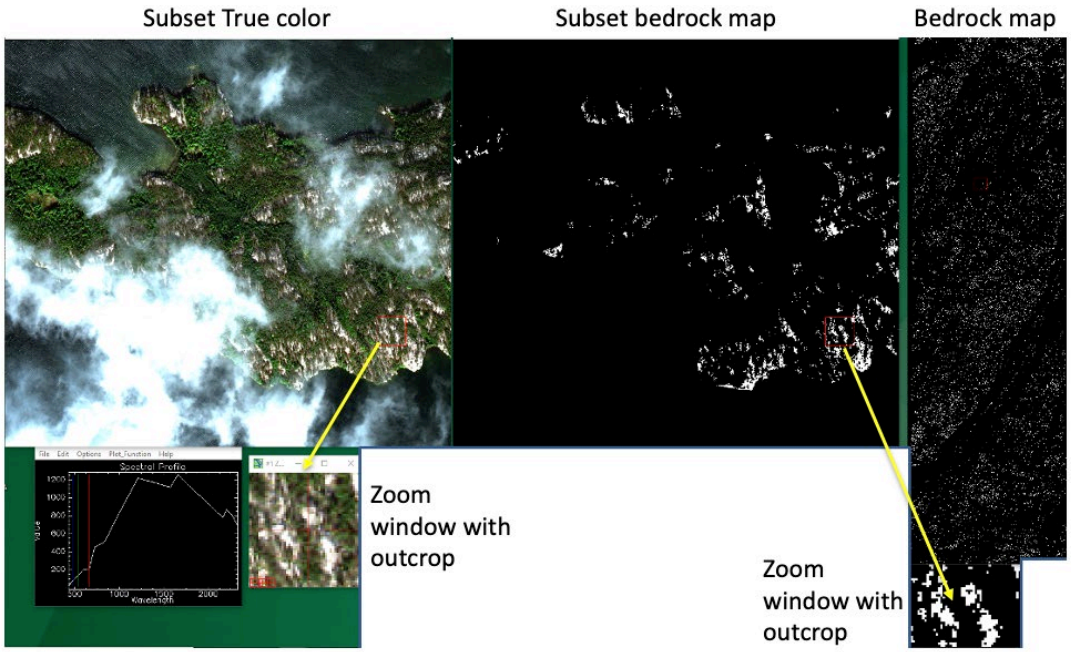


**Figure 6. Example of a portion of a generated outcrop map showing the impact of masking clouds, water, and vegetation via a comparison of a 'true colour' image with the final bedrock outcrop map product.**

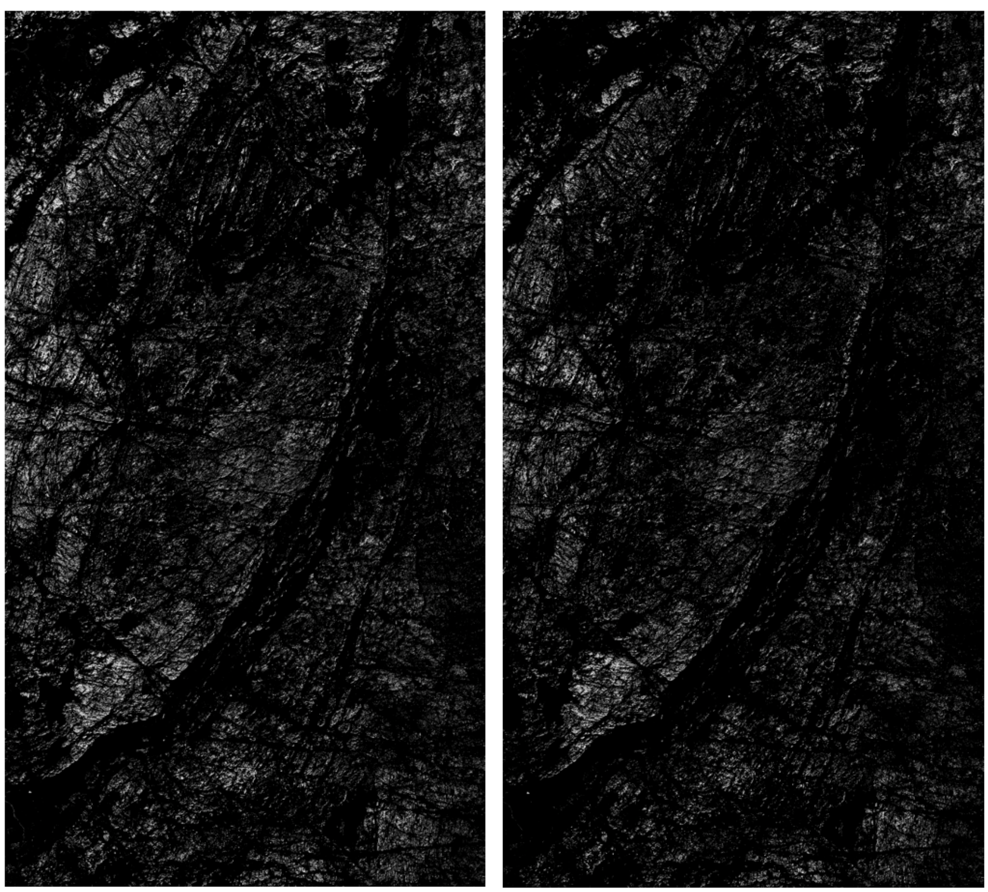

**Figure 7. Outcrop map (left) for planning fieldwork and that used for lithological analysis (right).**

## 4.2 Key endmember and index images

As part of the results, we present the suite of image products described in the ‘Methods’ section for a subset of the total area covered by imagery. We also make observations from these products in support of lithological inferences. An inherent challenge in the early stages of interpretation of such products is the environment that was imaged, which is partially forested and can lead to false image interpretations despite best efforts to remove the influence of vegetation in imagery. Another inherent challenge is the nature of the geology of the area, which has a predominance of felsic rocks that may display limited spectral diversity (e.g., similar mineralogy). Our approach for this report has thus been to focus on a region where the highest mapping detail was available, namely the Tulip Lake district, Sheet No. 34 at a scale of 1:31 680, published in 1984 (Godfrey and Langenberg, 1984) and shown in Figure 8. In doing so, we aim to establish potential correlations between map units and image domains and assign potential lithological labels to image observations with the recognition that such observations represent the early stages of image interpretation and are in need of field validation.

As stated by Langenberg et al. (1994), “the Leland Lakes area…exists along the Leland Lake shear zone, which is situated between the major Aphebian plutonic masses of the Slave granitoids in the west” (blue map units 101, 102, 103, 105 on Figure 8) “and the Arch Lake granitoids in the east” (brown map units 161, 162). “Other map units in the area are the Archean granite gneiss” (pink map unit 11) “and metasediments” (olive-green map unit 31). Amphibolites (pale green unit 20) occur in the area but are reported to be generally small in outcrop area and do not appear on the Tulip Lake map sheet. Below we suggest that some of the distribution of these units may be captured by the processed imagery. Figure 8 showcases the map legend and the map juxtaposed with the Rock MF (Mafic Felsic) image where Tulip Lake (letter A) and three rivers (B, C, D) are highlighted to provide the reader with common reference features. Note that the map and image are not coregistered but are at approximately the same scale. The reader can then compare the map (Figure 8) and varying image products (Figures 8 and 9) generated for lithological inferences.

The Rock MF index image (Figures 8 and 9D) was designed to contrast mafic and felsic rocks. For all images shown in Figures 8 and 9, the index values are displayed using a rainbow colour table, and in the case of the Rock MF image with red pointing to more mafic rocks and blue to more felsic ones. Figure 9A is a spectral angle map (SAM) generated using the endmember in Figure 4 with the highest reflectance (endmember 15) and is likely to represent the most felsic rocks. In this case, red is for the largest spectral angles, thus the greatest dissimilarity to the endmember. Figure 9B is the Rock Fe (iron) index image designed to detect the iron absorption in spectra with red showcasing the deepest absorption and, thus, the greatest abundance of iron oxide. Figure 9C is the White mica index that informs on the relative abundance of white mica with red colours representing a deeper hydroxyl absorption and thus a greater abundance of white mica. A cursory look may suggest similarity in imagery for A versus B and C versus D, but they each contain unique image domains. Amongst these four image products, several image domains are seen that may relate to established map units or add to existing ones as presented in the next section. These inferences presented below are preliminary requiring further analysis and field validation.

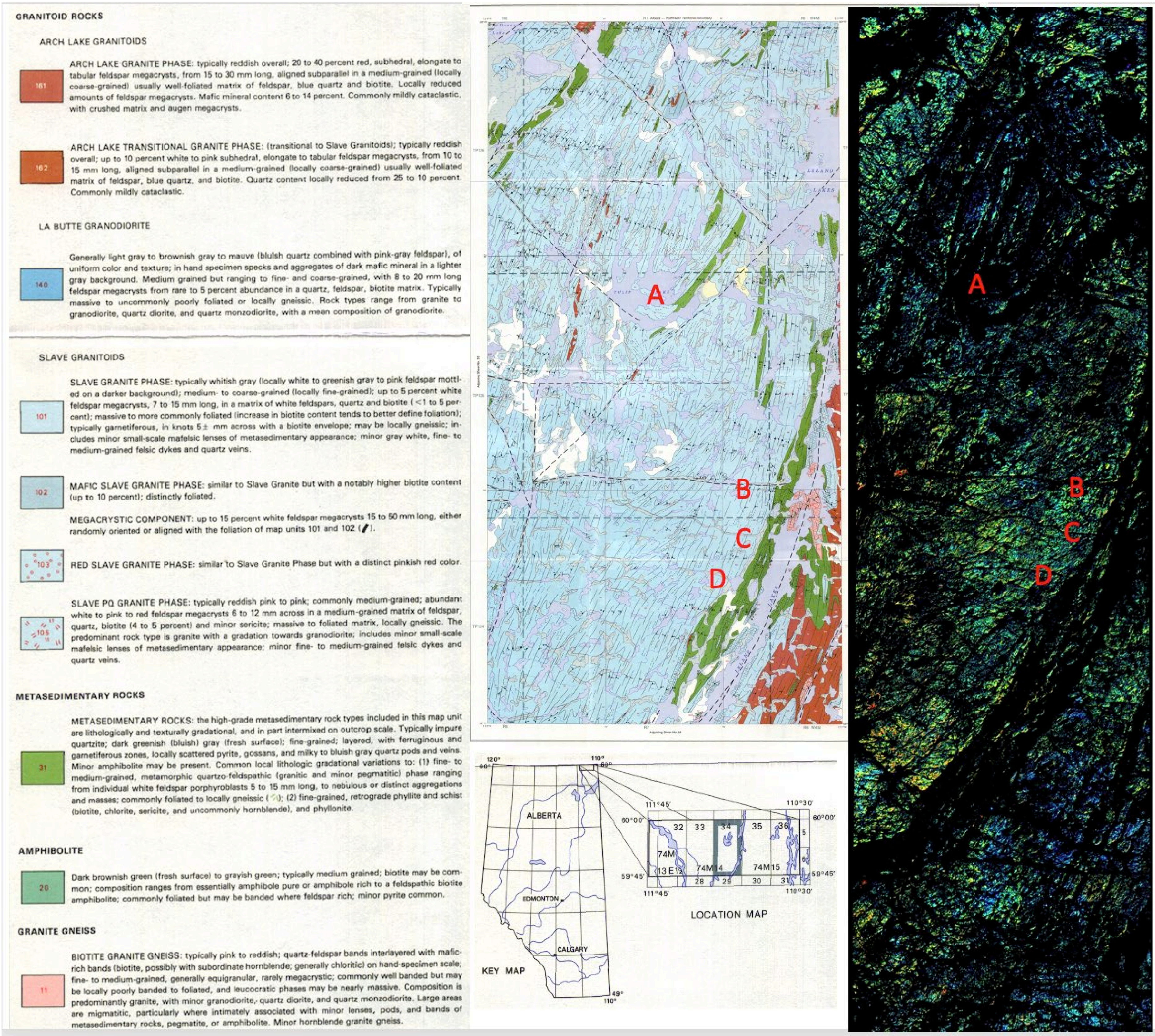


**Figure 8. Tulip Lake district, 1:31 680 scale, geological map (centre; Godfrey and Langenberg, 1984) along with legend (left) and the Rock MF index image (right). Tulip Lake (letter A) and three rivers (B, C, D) are highlighted on the map and image to provide the reader with common reference features.**

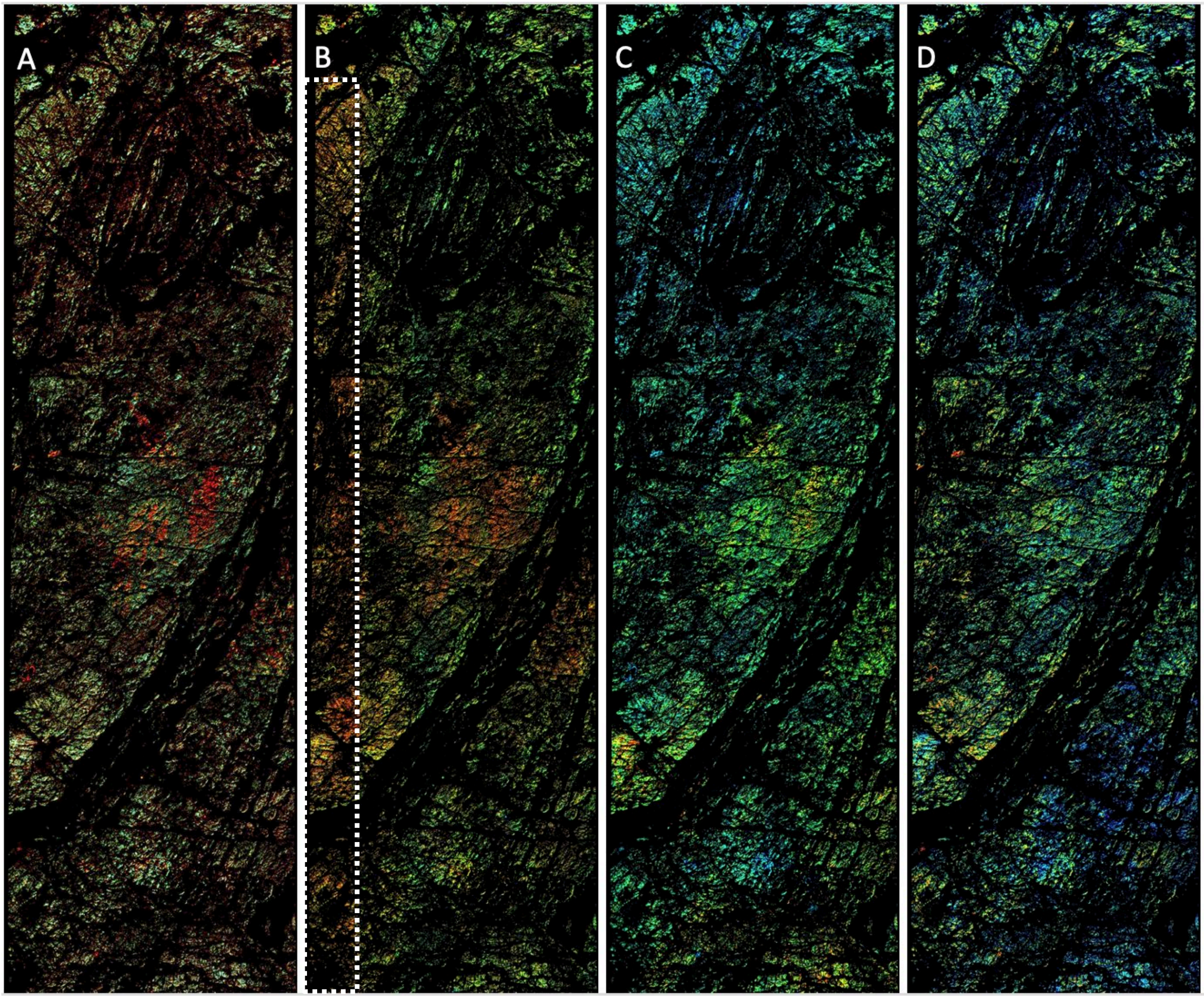


**Figure 9. Key endmember and index images: A) spectral angle map (SAM) generated using the endmember on Figure 4 with highest reflectance (endmember 15) where reds are for the largest spectral angles and thus the greatest dissimilarity to the endmember. B) Rock Fe (iron) index image designed to detect the iron absorption in spectra with red showcasing the deepest absorption and thus the greatest abundance of iron oxide. C) White mica index with red colours representing a deeper hydroxyl absorption and thus a greater abundance of white mica. D) Rock MF index image designed to contrast mafic and felsic rocks with red colours pointing to more mafic rocks and blue colours to more felsic ones. The dashed line polygon on the Rock Fe image highlights a portion of the image where misalignment artifacts are present (here as pervasive red hues throughout the polygon). Note that these are absent in the equivalent mosaic below (Figure 13).**

## 4.3 Possible links between map units and image domains

### 4.3.1 Observations for the southern half of the Tulip Lake map area

The following observations can be made when the southern half of the Tulip Lake map is juxtaposed with the Rock Fe and Rock MF index imagery (Figure 10). The portion south of Leland Lakes encompasses two dominant image domains (marked as '1' and '3' on Figure 10C). In comparison to domain 1, domain 3 is more felsic (blue on Rock MF index imagery) and displays less of an iron absorption (green versus red on Rock Fe index imagery; marked as '1' on Figure 10B). These observations are consistent with the descriptions of the two dominant map units in this region. The first being the Arch Lake granite phase and transitional phase (brown map units 161, 162), described as typically appearing reddish (e.g., iron oxide weathering of feldspar) in outcrop and with less than 14% mafics. Domain 1 appears to match the distribution of this granite phase. The second is the Slave granite phase (blue map unit 101), appearing whitish grey (e.g., more felsic, less iron rich) in outcrop and shown in the southern extremity of the map corresponding to domain 3. This suggests that the image products offer a means of distinguishing different felsic rocks.

North of Leland Lakes, the Tulip Lake map area consists almost exclusively of Slave granite phase (blue map unit 101) and metasediments (olive-green map unit 31). However, as seen in Figure 10 there is a suggestion, within the Slave granite phase map unit, of several domains (marked as '2' on Figure 10B) characterized by higher iron absorption (red on Rock Fe index imagery) alike the signature of the Arch Lake granite. Unlike the Arch Lake granite part of domain 2 (reddish domain in Figure 10C), these display a more pronounced hydroxyl feature (orange domain in Figure 9C). Based on observations in the lower half of the Tulip Lake map area, there may be at least two additional felsic units within the Slave granite phase map unit.

We also highlight in Figure 10B distinct domains captured by the Rock Fe index imagery (and possibly the White mica index) that appear to correspond with parts of the metasedimentary unit (olive-green map unit 31 and shown as 'Ms' on Figure 10B). It remains to be determined if a detection can be done in a consistent manner given the variable nature of metamorphosed metasediments. Their detection, though limited at this stage, is important given their relevance to exploration efforts as they host documented mineralization (Langenberg et al., 1994). Enhancement of the products targeting their detection is a recommended next step.

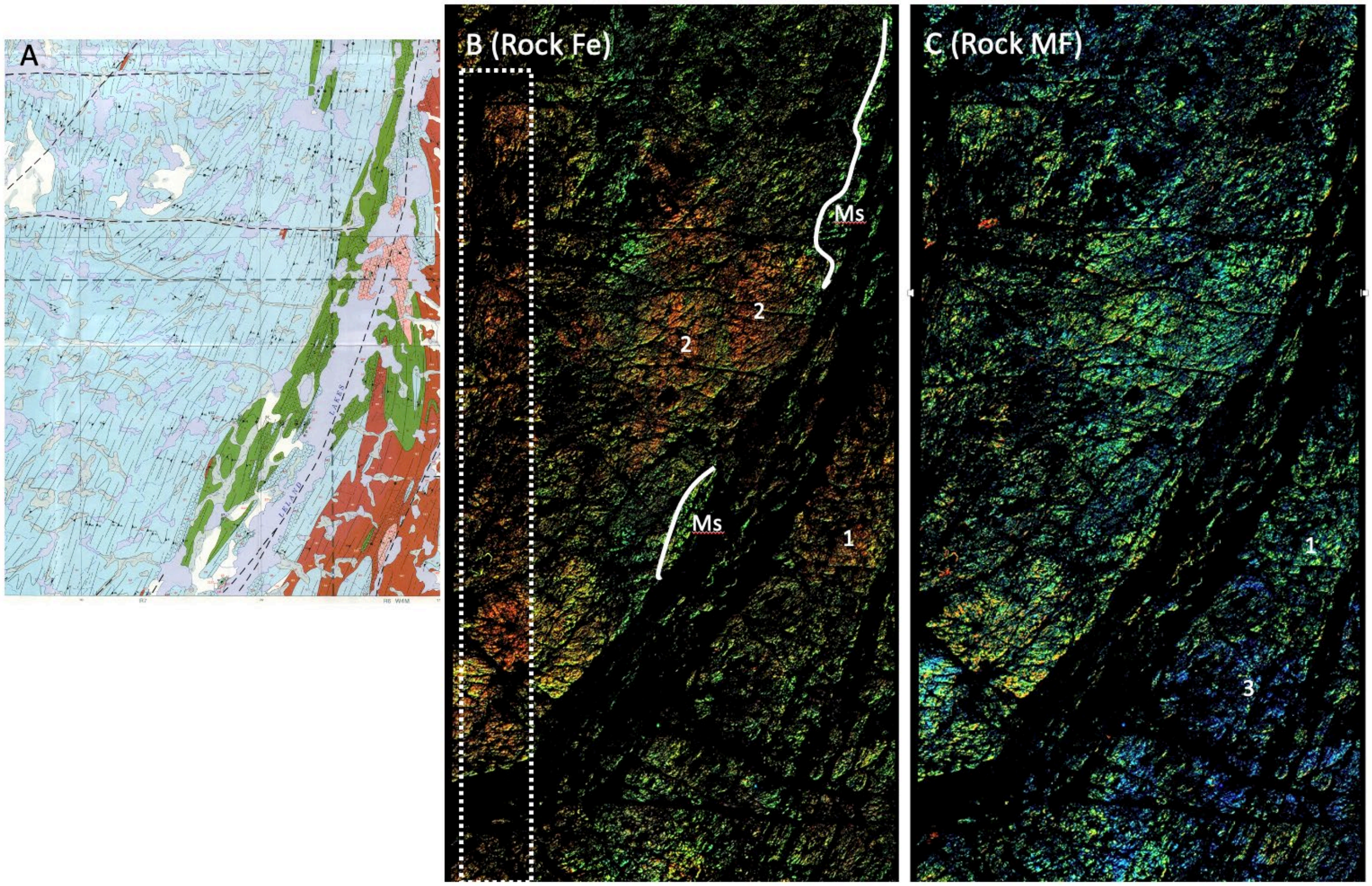


**Figure 10. The southern half of the Tulip Lake map area juxtaposed with the Rock Fe and Rock MF index imagery. Numbers 1, 2, and 3 refer to image domains discussed in the text. Ms refers to metasediments and the olive-green map unit 31.**

### *4.3.2 Observations for the northern half of the Tulip Lake map area*

Exposures of metasediments also appear to be captured by the Rock MF index image in the northern half of the Tulip Lake map area. As seen in Figure 11, white arrows on the Rock MF index image highlight narrow continuous red regions (more mafic). The three southernmost arrows appear to correspond to mapped metasediments (olive-green map unit 31), highlighted by red arrows on the map (Figure 11). These metasediments have a distinct appearance, with higher index values, thus more mafic, compared to the metasediments discussed in the previous section for the southern portion of the map area. This may point to a diverse set of spectral characteristics for this map unit as expected given the diverse mineralogical makeup of metasediments. Lastly it is worth pointing out that the central part of the Rock MF index image shown in Figure 11 encompasses a large area north of Tulip Lake with a predominance of blue pixels and was mapped as Slave granite (blue map unit 101). These may represent yet another unit within the Slave granite map unit, this one characteristically more mafic.

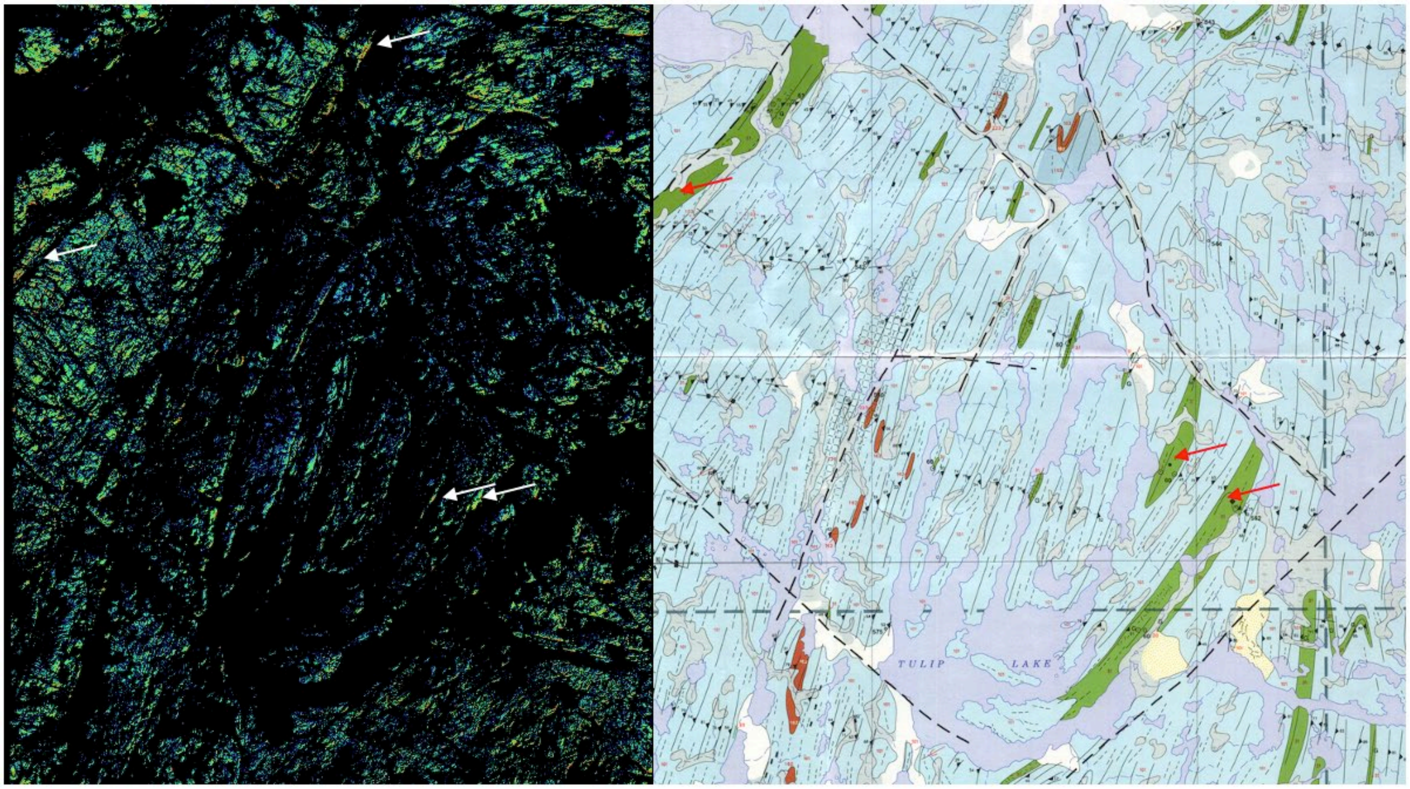


**Figure 11. The northern half of the Tulip Lake map area juxtaposed with the Rock MF index imagery. White arrows on the index image on the left highlight narrow continuous red regions (more mafic). The three southernmost arrows appear to correspond to mapped metasediments (olive-green map unit 31), highlighted by red arrows on the right.**

### 4.3.3 *Image composite for Tulip Lake map area and for the mosaic image of the area of interest*

An image product of potential value for visual analysis is a colour composite of the three index maps, as seen in Figure 12 for the Tulip Lake map area. This enhancement captures the observations described above in respect to variability within the Slave granite phase map unit and within the Arch Lake granite map unit. To help scale to the full region of interest, Figure 13 shows this composite, as well as the three index images (enhancements may differ slightly) for the mosaic. These reveal the full potential of the regional products that display many unique domains for each index. The White mica index map (Figure 13) shows a large domain in the southwestern corner of the mosaic, west of the Tulip Lake map area, which includes some of the strongest index values (e.g., high white mica abundance).

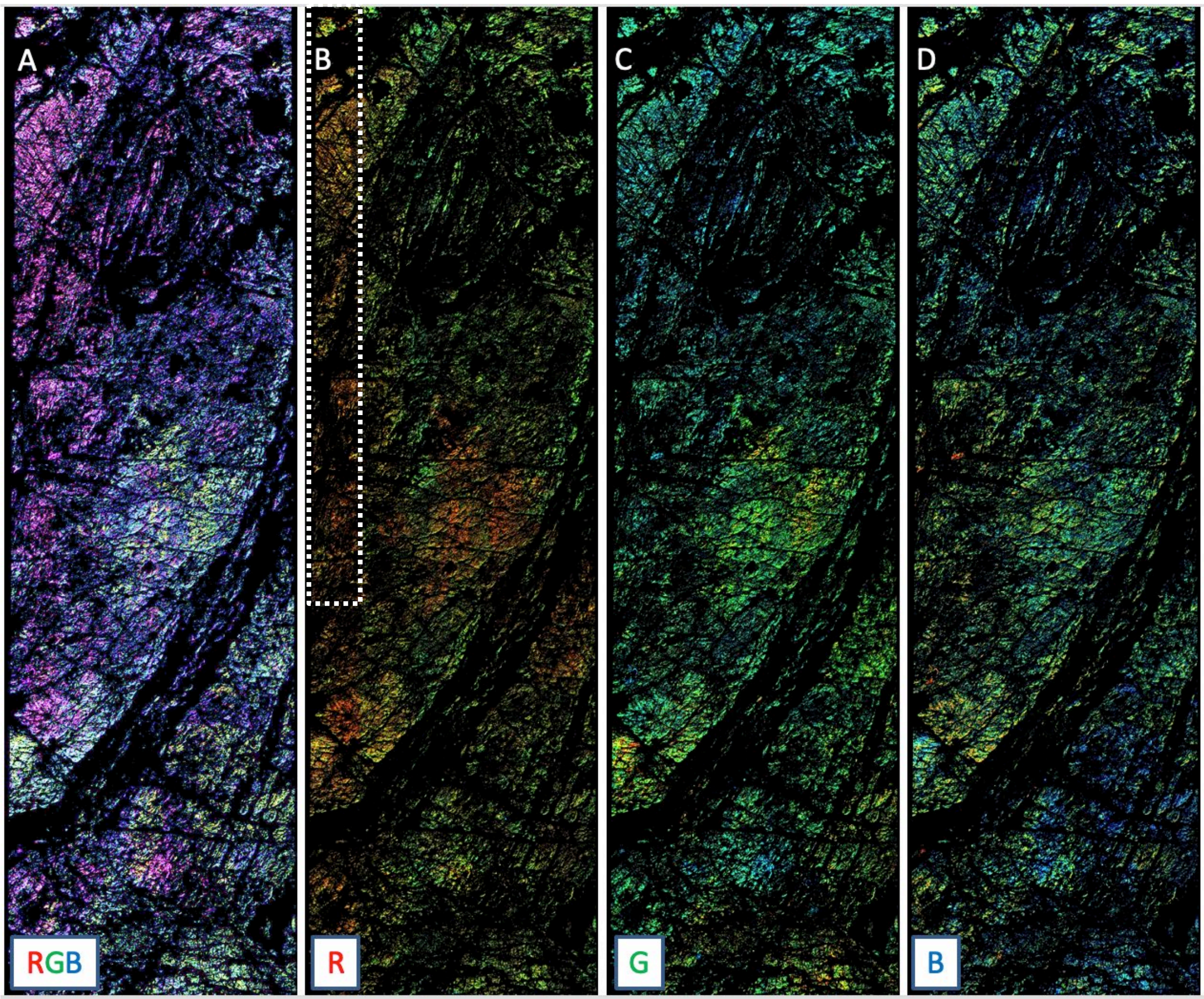


**Figure 12. Colour composite (A) of the three index maps for the single line encompassing the Tulip Lake map area: Red = Rock Fe index (B), Green = White mica index (C), and Blue = Rock MF index (D). The dashed line polygon on the Rock Fe index image highlights a portion of the image where misalignment artifacts are present.**

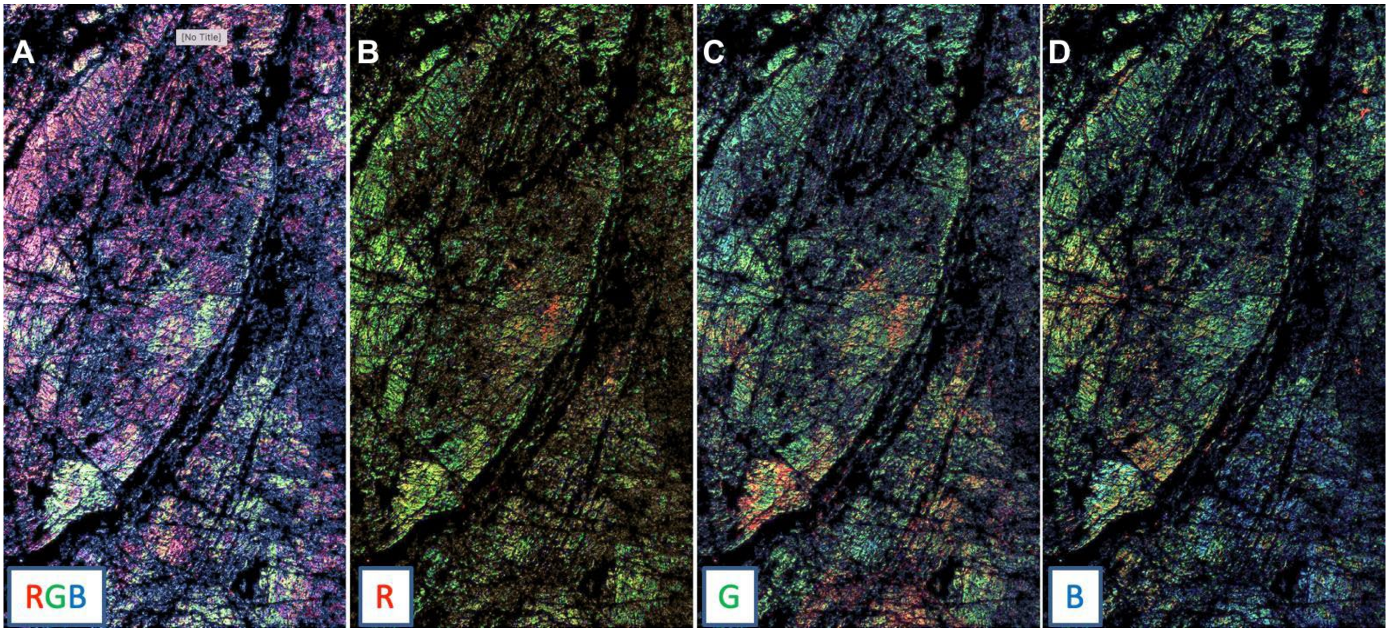


**Figure 13. Colour composite (A) of the three index maps for the mosaic covering the entire area of interest: Red = Rock Fe index (B), Green = White mica index (C), and Blue = Rock MF index (D).**

Lastly, we provide a colour composite of three spectral angle maps (SAM; Figure 14) generated using endmembers 1, 11, and 15 seen on Figure 4. Endmembers 1 and 15 are those of lowest and highest reflectance, respectively, and endmember 11 contrasts with these two in terms of spectral shape particularly between 900 and 1500 nm. Together they sample much of the variability seen amongst the 15 endmembers extracted using the full spectral dimensionality available (e.g., 16 bands). The current enhancement also captures the observations described above with respect to variability within the Slave granite phase map unit and with the Arch Lake granite map unit. It also captures the metasedimentary layer, highlighted in Section 4.3.1, in the northwestern portion of the Tulip Lake map area and shows its extension farther southwest.

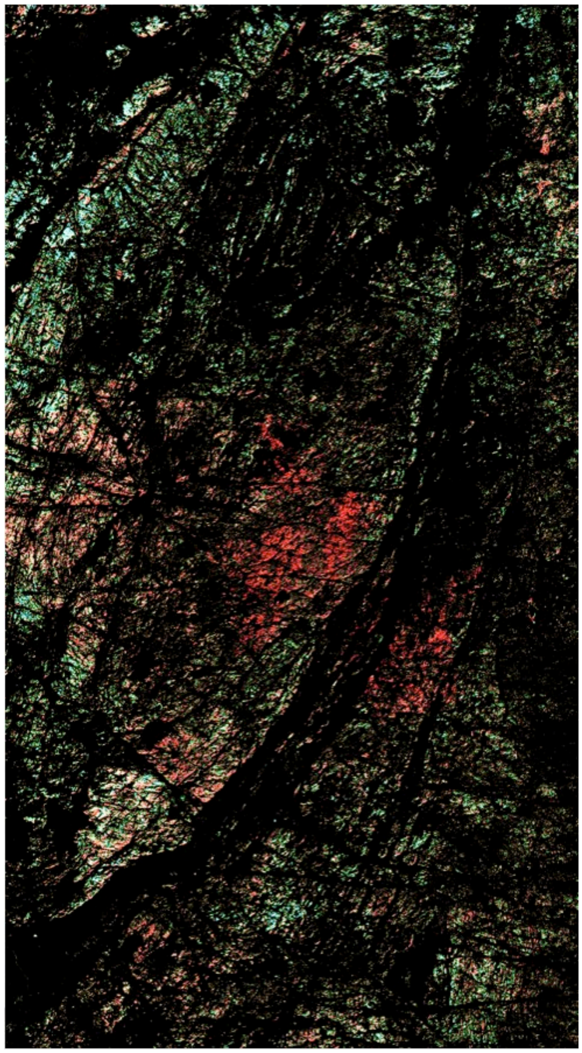

**Figure 14. Colour composite of three spectral angle maps (SAM) generated using endmembers 1, 11, and 15, seen on Figure 4. Red = endmember 15, Green = endmember 11, and Blue = endmember 1.**

# 5 DISCUSSION

## 5.1 Recommended use of map products for retrieval of geological information

As part of this initiative, considerable effort was spent preprocessing the data to isolate the portions of the scene occupied by outcrop and to minimize as best as possible the influence of vegetation and shadows. The benefit is that the spectral data encompassed by the ensuing outcrop map could be processed to reveal regional variability in the strength of absorption features of iron- and hydroxyl-bearing minerals. A preliminary analysis of three index images (Rock Fe, White mica, Rock MF) has begun to reveal a suite of felsic units and metasediments that appear to conform with the localized distribution of known map units in the Tulip Lake area, providing a first order validation. This represents the initial stage of the process of discovery of the data and this process is iterative. For example, we would suggest the continued exploration of all four image products shown in Figure 9 to fine-tune enhancements that assist in discerning the spectrally varying metasediments and the varying felsic (plutonic) rocks. For the former, this could be done while examining the links with reported gold, base metals, uranium, and rare-earth elements reported in narrow belts (Langenberg et al., 1994). One approach would be to define image domains, as per the examples discussed in this report, to produce a representative spectrum per domain and use it as an input into SAM to generate a spectral angle map that can be further enhanced to discern other domains. The SAM analysis may have to focus on subset spectral regions to capitalize on regional variability of iron or hydroxyl spectral features, since the imagery of related indices has revealed lithological information. This process is iterative and is intended to progressively reveal more subtle spectral differences with lithological significance. We suggest pursuing this iterative process first in the Tulip Lake map area, given the availability of a detailed map, and then scaling to the complete WorldView-3 image cover.

# 6 CONCLUSIONS

The limited spectral dimensionality of WorldView-3 imagery imposes serious constraints on the extraction of mineralogical information from satellite imagery, particularly in providing firm labelling of lithological inferences (e.g., mineral type as opposed to mineral groups). Nevertheless, the high spatial resolution has enabled the generation of an outcrop distribution map which should be of value for the planning of fieldwork. Considerable effort was spent preprocessing the data to isolate the portions of the scene occupied by outcrop and to minimize as best as possible the influence of vegetation and shadows. The benefit is that the spectral data encompassed by the ensuing outcrop map could be processed to reveal regional variability in the strength of absorption features of iron- and hydroxyl-bearing minerals. Lithological information is apparent from several related index images (iron, hydroxyl, mafic-felsic) and a felsic endmember SAM image after careful removal of pixels occupied by water, clouds, shadows, and vegetation to only retain the 'cleanest bedrock' pixels.

A preliminary analysis of these four images reveals a suite of felsic units and metasediments that appear to conform with the localized distribution of known map units in the Tulip Lake area, providing a first order validation of the interpretations. Despite the challenging settings for lithological remote sensing (e.g., vegetated terrain and predominance of felsic rocks), the image products generated from the analysis of WorldView-3 imagery offer value for the planning of field activities, with further value to be unlocked through iterative analysis.

# 7 REFERENCES

Godfrey, J.D. and Langenberg, C.W. (1984): Geology of the Tulip Lake district, Alberta; *in* Geology of the Fitzgerald, Tulip-Mercredi-Charles Lakes District, Alberta, Alberta Research Council, Alberta Geological Survey, Earth Sciences Report 84-7, scale 1:31 680.

Langenberg, C.W., Salat, H.P. and Eccles, D.R. (1994): Mineral occurrences of the Selwyn and Leland Lakes areas, northeast Alberta; Alberta Research Council, Alberta Geological Survey, Open File Report 1994-5, 26 p.

Price, J.C. (1994): How unique are spectral signatures?; Remote Sensing of Environment, v. 49, p. 181–186.

Rogge, D., Bachmann, M., Rivard, B. and Feng, J. (2012): Spatial sub-sampling using local endmembers for adapting OSP and SSEE for large-scale hyperspectral surveys; IEEE Journal of Selected Topics in Applied Earth Observations and Remote Sensing, v. 5, p. 183–195.

Rogge, D., Rivard, B., Zhang, J., Harris, J., Feng, J. and Sanchez, A. (2007): Integration of spatial-spectral information for the improved extraction of endmembers; Remote Sensing of Environment, v. 110, no. 3, p. 287–303.

Shedlovska, Y.I. and Hnatushenko, V.V. (2019): Shadow removal algorithm for remote sensing imagery; IEEE 39th International Conference on Electronics and Nanotechnology (ELNANO), p. 818–822, doi:10.1109/ELNANO.2019.8783642.

## APPENDIX 1: List of digital deliverables

Georeferenced mosaic data for the following products are provided in ENVI format and in Geotiff format for visually enhanced products. JPG formatted files are also available for quick view.

| Product | File name | Number of files |
|---|---|---|
| 1) Mosaic of WV3 data, 16 bands | WV3-Mosaic_Leland_Lakes | 1 (envi) |
| 2) Outcrop map | LelandL_Outcrop | 2 (envi, geotiff) |
| 3) SAM map of endmembers 1,11,15 | LelandL _SAM_RGB | 3 (envi, geotiff, rule) |
| 4) Rock FE index image | LelandL _Rock Fe | 2 (envi, geotiff) |
| 5) White mica index image | LelandL _OH | 2 (envi, geotiff) |
| 6) Rock MF index image | LelandL _Rock_MF | 2 (envi, geotiff) |
| 7) Endmember spectra library | LelandL_rockEM | 1 (envi) |

# APPENDIX 2: Mosaic images seen in Figure 13

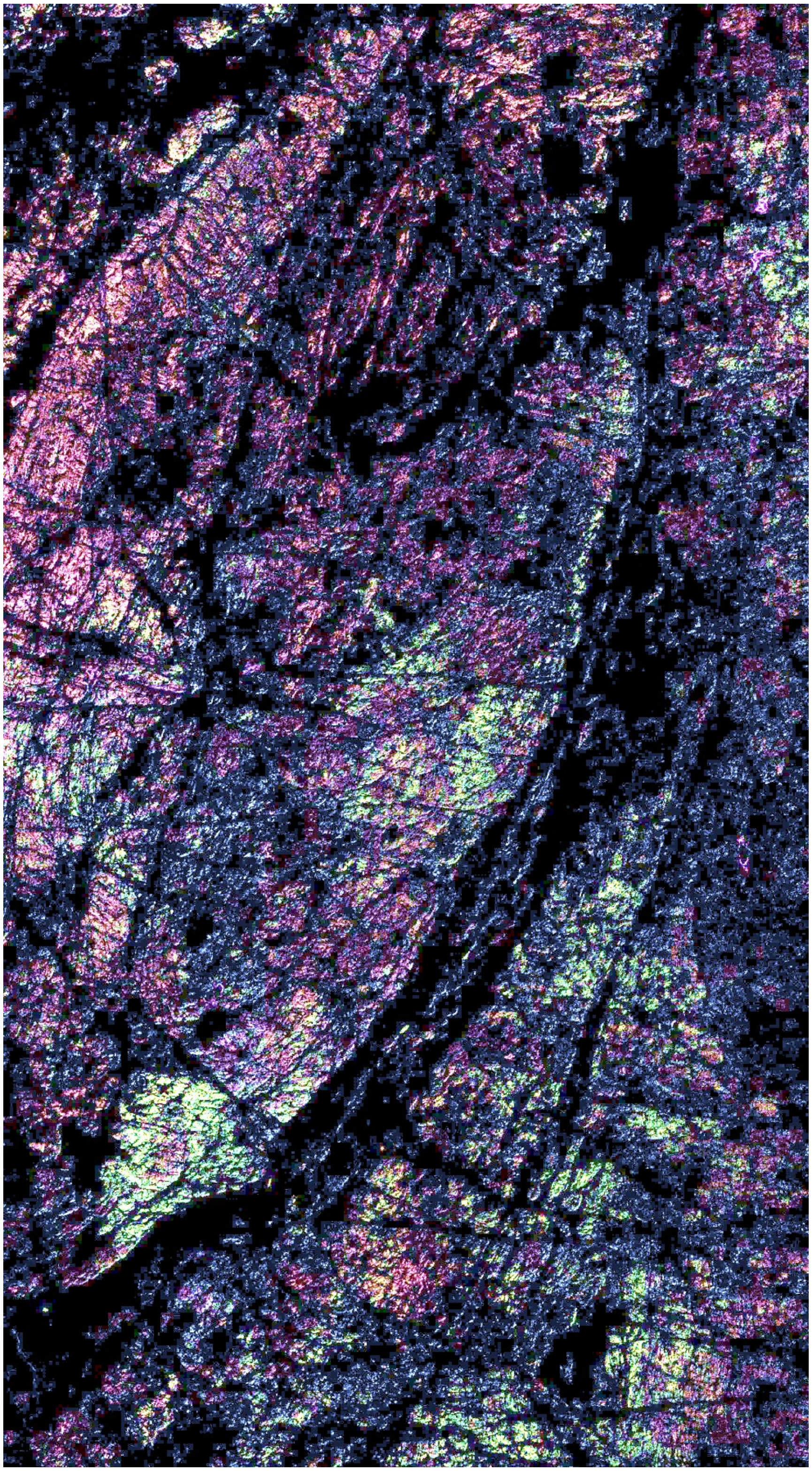

**Figure 15. Enlargement of colour composite shown in Figure 13A.**

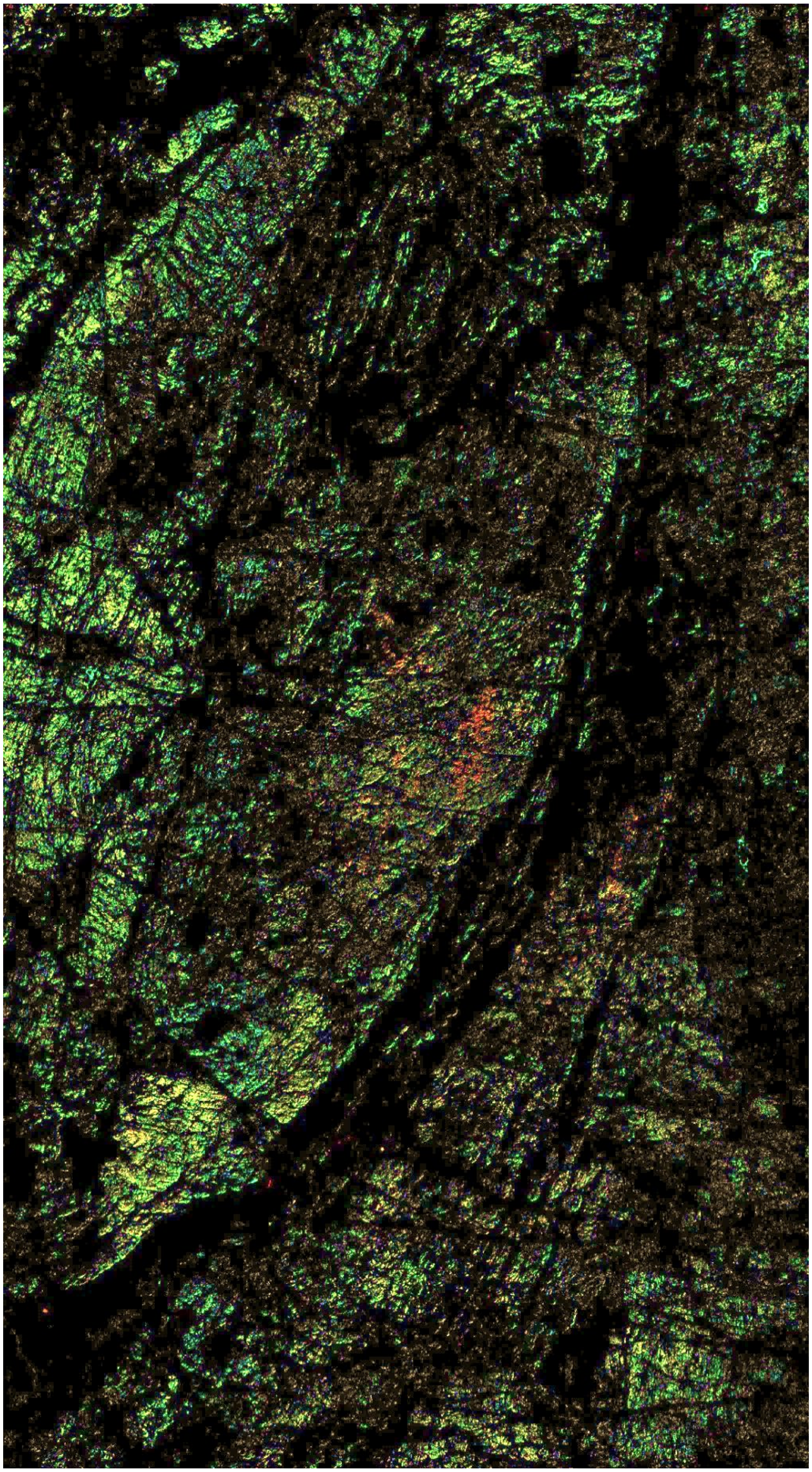

**Figure 16. Enlargement of Rock Fe index image shown in Figure 13B.**

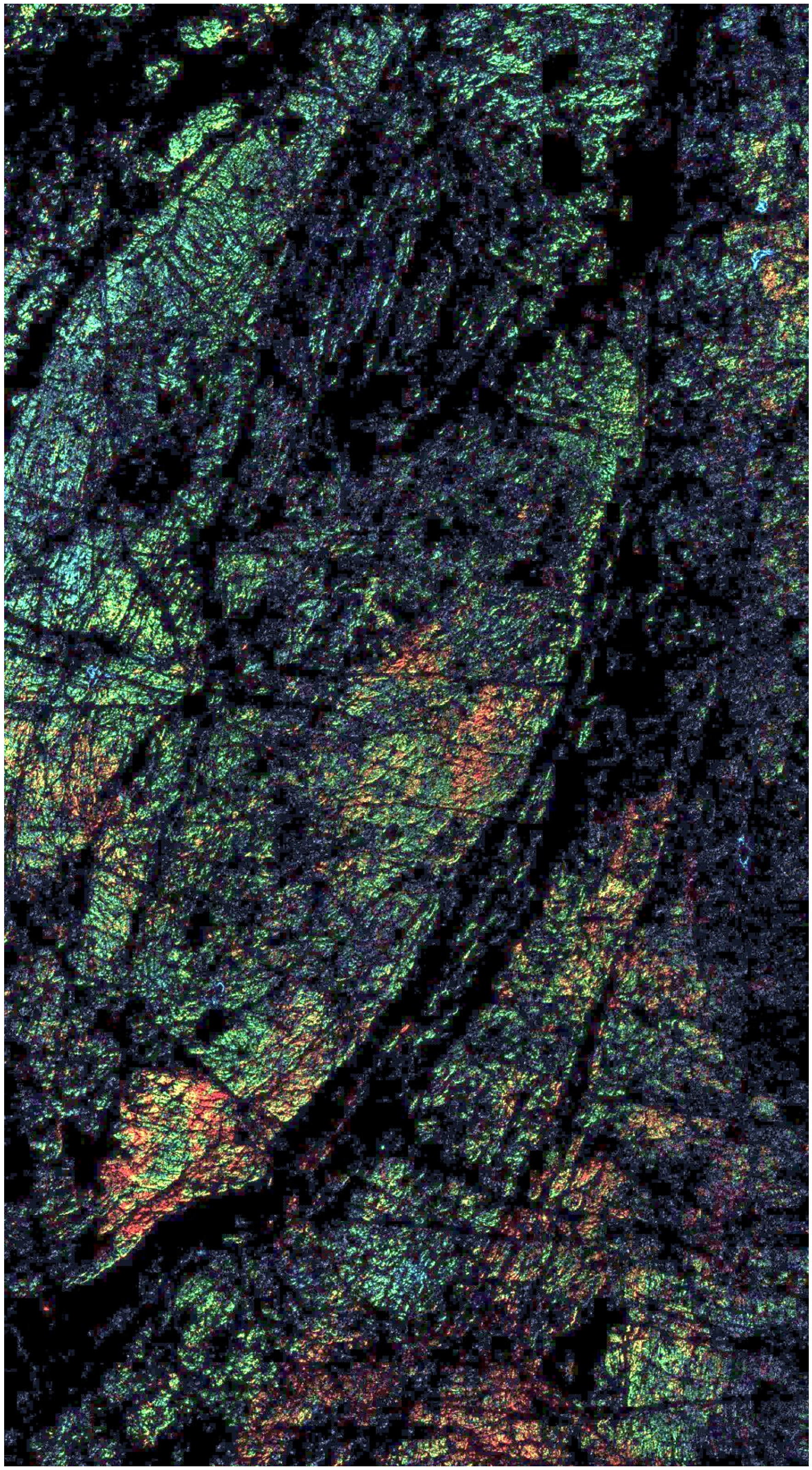

**Figure 17. Enlargement of White mica index image shown in Figure 13C.**

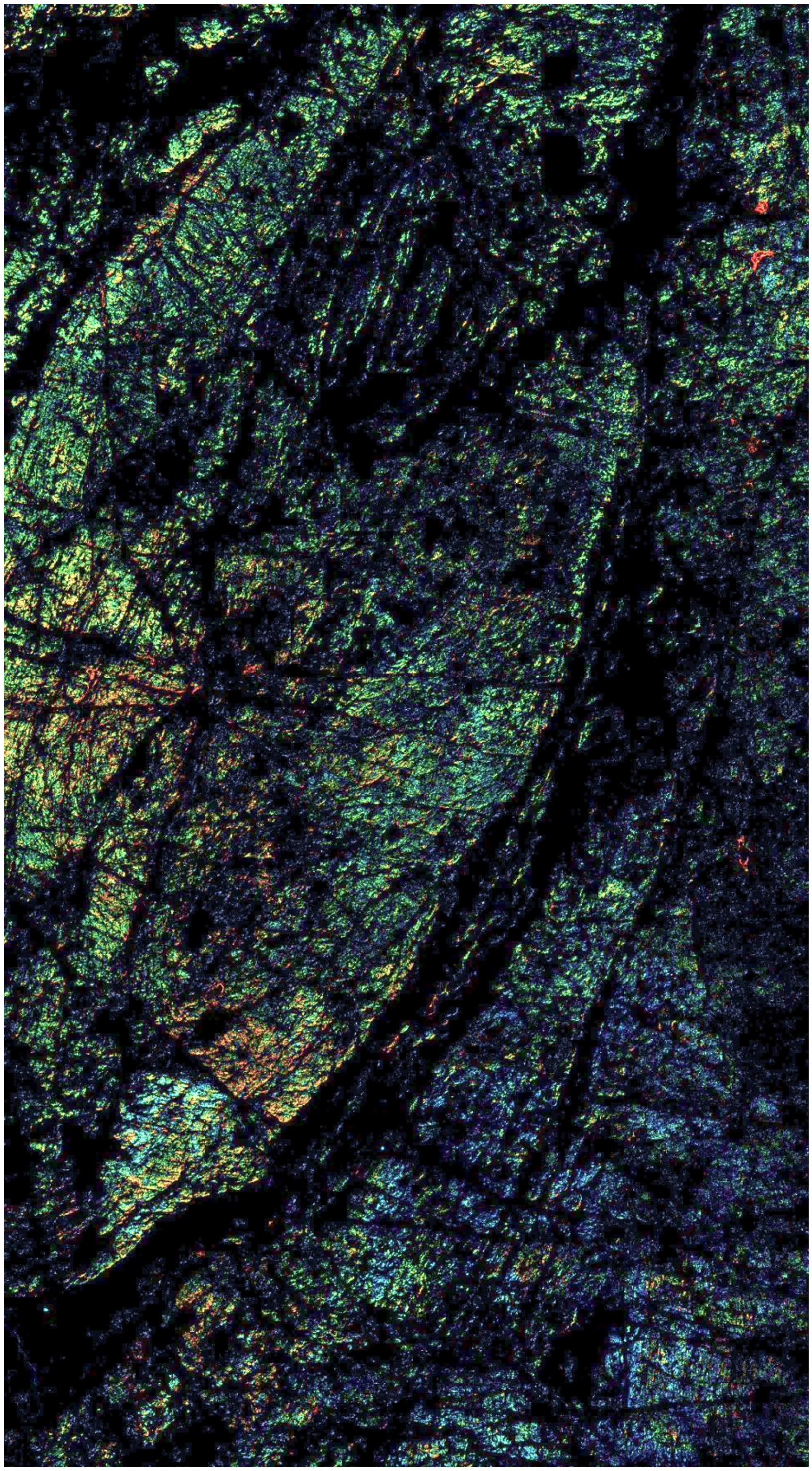

**Figure 18. Enlargement of Rock MF index image shown in Figure 13D.**